Journal of Testing and Evaluation, Vol. 35, No. 6
Paper ID JTE100598
Available online at: www.astm.org

Joy P. Dunkers,[1] *Stefan D. Leigh,*[2] *David Dean,*[3] *Malcolm N. Cooke,*[4] *Richard A. Ketcham,*[5] *and Marcus T. Cicerone*[6]

Methodology for Evaluating Candidate Geometric Reference Scaffolds*

ABSTRACT: Along with the ASTM Division IV subcommittee on Tissue Engineered Medical Products, the National Institute of Standards and Technology is developing a geometric reference scaffold. This paper describes the methodology applied to the three different types of candidate reference scaffolds to quantify their structure and rank them according to quality metrics. In this work, we detail this methodology using the candidate reference scaffold produced by stereolithography. We perform X-ray micro-computed tomography on three of the manufactured scaffolds and compute total porosity, pore size distribution, and pore length for each. We compare these quantities to those of the model scaffold using statistical measures of variational distance, relative uncertainty, and uniformity. Through this evaluation, we find that the scaffold produced by stereolithography agrees well with its model and merits further consideration as a reference scaffold.

KEYWORDS: tissue engineering, reference scaffold, geometry, structure, pore volume, pore length, variational distance

Introduction

In functional tissue engineering, the ability of scaffolds to support the development of tissues depends on many properties that encompass the areas of scaffold geometry, mechanical properties, topography, and chemistry. Two National Institute of Standards and Technology (NIST) workshops in 2000 [1] and 2001 [2] identified reference scaffolds as filling a critical need for referencing measurements that characterize scaffolds and the responses of cells and tissues to them. One of the conclusions drawn from the 2000 workshop is that "the reference materials most needed are three-dimensional reference tissue scaffolds of known porosity, interconnectivity, surface and bulk chemistry, physical and mechanical properties, and cellular reactivity" [1].

At the November 2003 meeting, ASTM Division IV (Standards for Medical and Surgical Materials and Devices) formed a task force (F04.42.06) to initiate the development of reference scaffolds for the characterization of porosity [3]. The outcome of the meeting was that two types of cubic polymer test scaffolds, one manufactured by 3-D microprinting [4] and the other by stereolithography [5], having 300 μm and 600 μm pores would be fabricated and distributed to those groups participating in the task force for characterization. Another type of polymer scaffold made by fused deposition modeling was added later [6]. Samples of each scaffold type were distributed to the task force which characterized their structure using X-ray micro-computed tomography, scanning electron microscopy, magnetic resonance imaging, and Brunauer-Emmett-Teller surface area and roughness measurements. The results were presented at the May 2005 ASTM meeting to the subcommittee on tissue engineered medical products. Based on the results from the task force, one type of scaffold was selected for further evaluation based on its chemical composition and structural uniformity and reproducibility, which was attributed to its manufacturing method.

Rapid prototyping (RP) methods, such as those mentioned above, are well suited for manufacturing reference scaffolds since they can be used to fabricate solid polymer scaffolds with simple, regular, and repeatable geometries, pore structures, connections, and interconnections. The phrase "solid freeform fabrication" has been used interchangeably with RP to encompass all the techniques that generate a controlled architecture. Four recent papers on RP techniques have done an excellent job of summarizing how each RP technique functions, its feature size, advantages and disadvantages, and its ability to incorporate cells and other biological factors [7–10]. The most recent advance in RP is the use of multi-photon excitation to tightly control scaffold feature size to the order of the size of focal contacts. Using this method, features from several hundred nanometres up to 1 μm were fabricated [11].

Some techniques traditionally used to quantify scaffold structure include scanning electron microscopy, mercury and flow porosimetry, gas adsorption, and pycnometry [12]. These techniques probe a limited number of descriptors of interest—most commonly porosity, pore size distribution, tortuosity, surface area, permeability, and compressibility—with caveats. The biggest drawback to all of the techniques is that they do not provide a direct measure of scaffold structure in three dimensions. X-ray micro-computed tomography (micro-CT) provides a direct measure of scaffold structure and has been used to generate 3-D images of scaffolds [13,14]. There have been several efforts to quantify the results from using this technique for both scaffold structure [12,15] and mineralization within bone tissue constructs [16,17]. In this work, we will use

Manuscript received April 19, 2006; accepted for publication April 24, 2007; published online June 2007.

[1]Physical Scientist, Polymers Division, National Institute of Standards and Technology, Gaithersburg, MD 20899-8543
[2]Mathematician, Mathematical and Computational Sciences Division, NIST, Gaithersburg, MD 20899-8980
[3]Associate Professor, Department of Neurological Surgery, Case Western Reserve University, Cleveland, Ohio 44106
[4]Assistant Professor, College of Engineering, University of Texas at El Paso, El Paso, TX 79968
[5]Senior Research Scientist, Jackson School of Geosciences, University of Texas at Austin, Austin, TX 78712-0254
[6]Group Leader, Polymers Division, NIST, Gaithersburg, MD 20899-8543

*Official contribution of the National Institute of Standards and Technology (NIST); not subject to copyright in the United States.

Copyright © 2007 by ASTM International, 100 Barr Harbor Drive, PO Box C700, West Conshohocken, PA 19428-2959.

micro-CT to generate images of one candidate reference scaffold manufactured using stereolithography.

The motivation for the work is to rank candidate reference scaffolds by quality metrics in a systematic and quantitative manner by screening several microstructural descriptors of importance. We chose total pore volume, pore volume distribution, and pore size distribution as the descriptors of interest for statistical analysis. The goal of this paper is to establish a methodology to answer the following: (1) How accurately do the fabricated scaffolds replicate the model? (2) How uniform in structure are the fabricated scaffolds? We describe the process by which these questions are addressed for the Type 1 candidate reference scaffolds provided by Dean and Cooke at Case Western Reserve University. First, we built a model scaffold using a computer aided design (CAD) template. This is our ideal structure to which the manufactured parts are to be compared. Second, we derived theoretical values for the pore volume and pore size from known unit cell dimensions. We next performed a quantitative 3-D image analysis on the model scaffold to evaluate any bias the analysis itself may have introduced. We then performed 3-D image quantitation on the image sets taken using micro-CT from three scaffolds manufactured using stereolithography. The pore volume and pore size distribution were compared to the model using a statistic called variational distance [18]. The results of such an analysis enable us to score and rank the test scaffolds according to how accurately they replicate the model. We also provide a score for scaffold uniformity for each metric. The 3-D structure quantitation performed by NIST on Types 1, 2, and 3 of the candidate scaffolds is published elsewhere [19].

Experimental

Scaffold Fabrication

The Type 1 candidate reference scaffolds were fabricated using a 3-D Systems' Viper SLA[7] machine which consists of a servomechanism to control the beam of a solid-state UV laser in the X and Y horizontal axis, a tank containing a liquid monomer resin, and a motorized build table that travels vertically in the Z axis up and down in the resin tank. The CAD model is first sliced into layers by preprocessing software (i.e., 3-D Systems' Lightyear) and the data are downloaded to the Viper SLA machine. The layer profile data are used to control the laser. When the beam focuses on the resin surface, it causes the resin to polymerize. The build table is lowered into the liquid Accura si 10 resin one-layer thickness at a time after each layer has been polymerized to construct the final object. Sample numbers 2, 4, and 17 were randomly selected for analysis from the sample set.

Micro-CT

The micro-CT images were generated by a Skyscan 1072 micro-computed tomography scanner with a 1024 by 1024 pixel camera. A current of 0.1 mA, operating voltage of 40 kV, and integration time of 1900 ms were used to acquire the images. Two hundred projections were generated and reconstructed using the Feldcamp algorithm. In all cases, the voxel size was 11.26 μm. Each dataset was output as individual 2-D bitmap files. In this work, the dominant error is a Type B standard uncertainty originating from the resolution limit of the instrument and is estimated to be 3.2 %.

[7]Certain commercial equipment, instruments, or materials are identified here to adequately specify experimental procedure. Such identification is not intended to imply recommendation or endorsement by NIST, nor does it imply that the materials or equipment identified are the best available for the purpose.

Quantitative Image Analysis

Using MATLAB, the bitmap files were cropped and output as tiffs for image quantitation. A three-dimensional image analysis package called Blob3D was used to extract pore length distribution and pore volume distribution for the CAD model scaffold and for the micro-CT imaging data for all scaffolds. The software was written by Ketcham using Interactive Data Language (IDL, Research System, Inc.) [20] and is designed for extracting morphological information on up to thousands of individual features within large three-dimensional datasets.

Blob3D takes a stack of 2-D bitmap or tiff images, along with the within-slice pixel dimension and between-slice spacing, as inputs to reconstruct the 3-D volume. For this application, the pores were segmented using one repeat of a median filter with a kernel radius of two pixels. To set a threshold value of each dataset, the histogram of an image plane that vertically bisects the pores of three randomly selected rows is displayed. All histograms are the same qualitatively and have a clear bimodal distribution of intensities with a consistent distance between the two peaks, about 120 ± 3. The threshold value is set at 50 % of the distance between the two peaks and the images were converted to binary. Next, the software separates features by performing repeated erosion and dilation operations, all the while retaining information on the starting pixel locations. In this work, the separated pores are called unit cells because of their well defined nature. For each unit cell, pore volume (PV) was measured by counting the number of voxels encompassing the pore and multiplying by the voxel dimension. Pore length (PL) was approximated as the long axis of the best-fit ellipsoid to the unit cell surface. The ellipsoid short axis was also recorded, along with the object coordinates.

The main descriptors that one addresses in relation to cell response are total pore volume, otherwise known as porosity, and pore size distribution. Other more sophisticated descriptors are pore connectivity, size of connections in between pores, tortuosity, and curvature, permeability, and anisotropy. Because the method in this paper is developed to screen the candidate reference scaffolds for selection, total pore volume and pore size distribution were selected. Pore volume distribution is also used because it is seen to be more reliable than pore size distribution, calculated by counting voxels rather than by the length of the major axis to an ellipsoid fit. Because the architecture is very regular and not random like many scaffolds created by leaching porogens, more sophisticated metrics described above were not needed.

Statistical Analysis

Variational Distance—To assess relative goodness-of-fit between scaffold specifications and experimental measurements on scaffolds, a metric is required. A standard approach to testing goodness-of-fit to a prespecified distributional form is to employ a chi-square analysis. Application of chi-square requires binning of the empirical comparison distribution, with a substantive number of bins for which actual comparisons can be made. That is not the case here since the pore diameter distribution consists of two modes and the pore volume distribution consists of four modes.

Also, the empirical image analysis estimates of both distributions are quite diffuse with poorly defined spikes offset from where the nodes should actually be.

A more appropriate statistical measure is the variational distance between two discrete densities, or probability mass functions (pmfs) defined as:

$$d = \frac{1}{2}\sum_{k=0}^{\infty} |P(X=k) - P(Y=k)| \quad (1)$$

where the random variables X and Y represent an ideal pmf for volume or diameter of a scaffold. This can be illustrated as a histogram representation of empirical pmf measurements on a manufactured realization of the same scaffold. The formula defines a true distance. It takes on values between 0 and 1, is symmetric in its arguments, X and Y, and satisfies a triangle inequality.

We adapt this metric here to the comparison of discrete densities with arbitrary support. We want to compare ideal pore volume and pore diameter densities to empirical (histogram) estimates of the same. We adapt the definition of variational distance by enforcing, for any specific ideal-to-experimental comparison, a fixed binning scheme on both ideal and empirical densities, and computing the obvious analog of the variational distance:

$$d = \frac{1}{2}\sum_{bin} |P(X \text{ in } bin) - P(Y \text{ in } bin)| \quad (2)$$

This formula is easily implemented in code. For this paper, we use DATAPLOT, public domain statistical analysis software developed at NIST [21].

The application of the formula, for example, to the comparison of measurements of parts 2, 4, and 17 of the Type 1 scaffold against its ideal volume distribution readily lead, for binning scheme (lowest bin lower boundary 0.0, bin width 0.1, highest bin highest boundary 1.4) to values 0.07 (part 4) $<$0.14 (part 17) $<$0.16 (part 2), giving a natural ordering for these (Type 1) parts. Lower values of the empirically estimated variational distance correspond to better fits against the ideal(s).

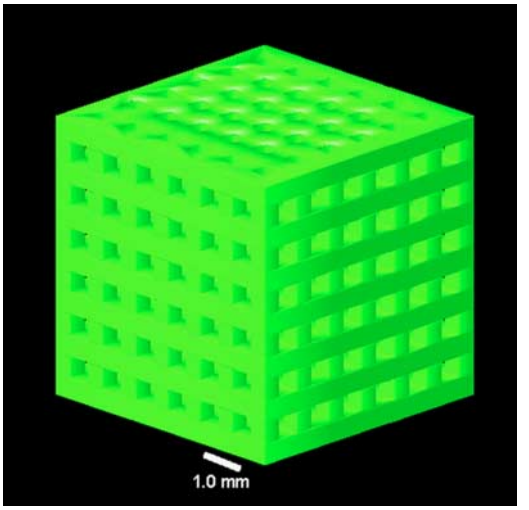

FIG. 1—*Type 1 reference scaffold reconstructed from CAD template.*

To sharpen the comparison between variational distances, we use a bootstrap to estimate their standard errors. Bootstrapping is a generic technique for computing uncertainties. It consists of repeated Monte Carlo resampling from an original single dataset, applying a data reduction process, and then computing the uncertainty from the multiply recomputed values. It is somewhat counterintuitive that a good estimate of the true sampling distribution of a statistic could be obtained from a single sample. Yet, the bootstrap estimates, which have now been constructed and tested for a wide variety of statistical procedures, can be shown to have excellent theoretical properties [21,22].

Bootstrapping in this context amounts to repeatedly resampling with replacement a set of multiple pore volume measurements, forming in each instance the histogram according to prespecified binning (same for both ideal and empirical), computing the dis-

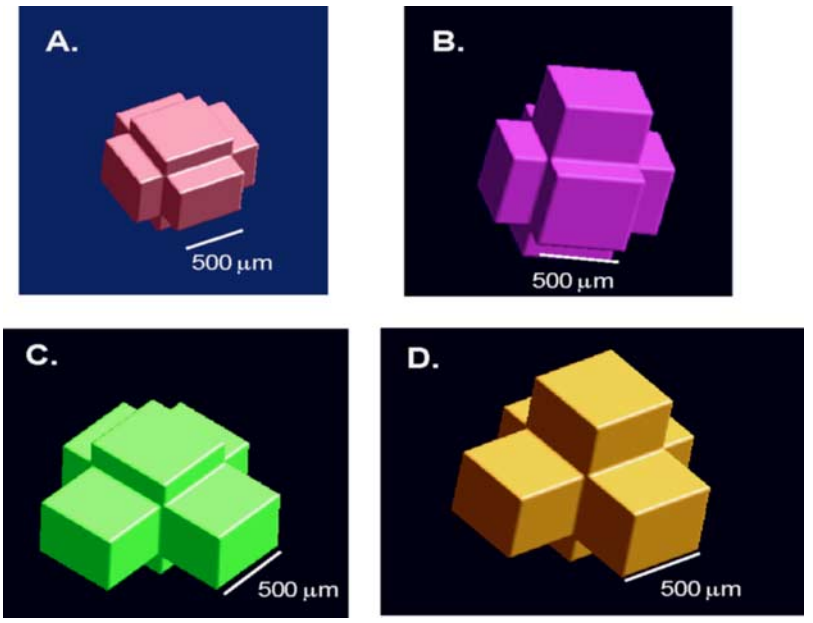

FIG. 2—*Four unit cells (UCs) found in the Type 1 reference scaffold. Each UC is found in a specific location in the scaffold: Interior (A), Face (B), Edge (C), and Corner (D).*

TABLE 1—*Comparison of the theoretical and model derived values for the four unit cells for the Type 1 scaffold.*

	Theoretical Values				Model Derived Values			
	A	B	C	D	A	B	C	D
Number of unit cells in scaffold	64	96	48	8	64	96	48	8
Average PV (mm^3) ($\pm 8 \times 10^{-6}$ mm^3 for model derived)	0.756	0.846	0.936	1.026	0.756	0.855	0.948	1.041
Average PL (mm) (±0.020 mm for model derived)	1.1	1.35	1.35	1.35	1.20	1.46	1.46	1.46

tance, and iterating 200 times. The desired standard error is the standard deviation of the resulting set of 200 variational distances. Doing this for the Type 1 parts yields 0.07±0.02, 0.14±0.03, and 0.16±0.04 as estimates for the variational distances and standard errors for parts 4, 17, and 2, respectively.

As might be expected, the computed variational distances are sensitive to the chosen binning scheme. It is desirable that orderings be invariant to the choice of binning scheme. So, for example,

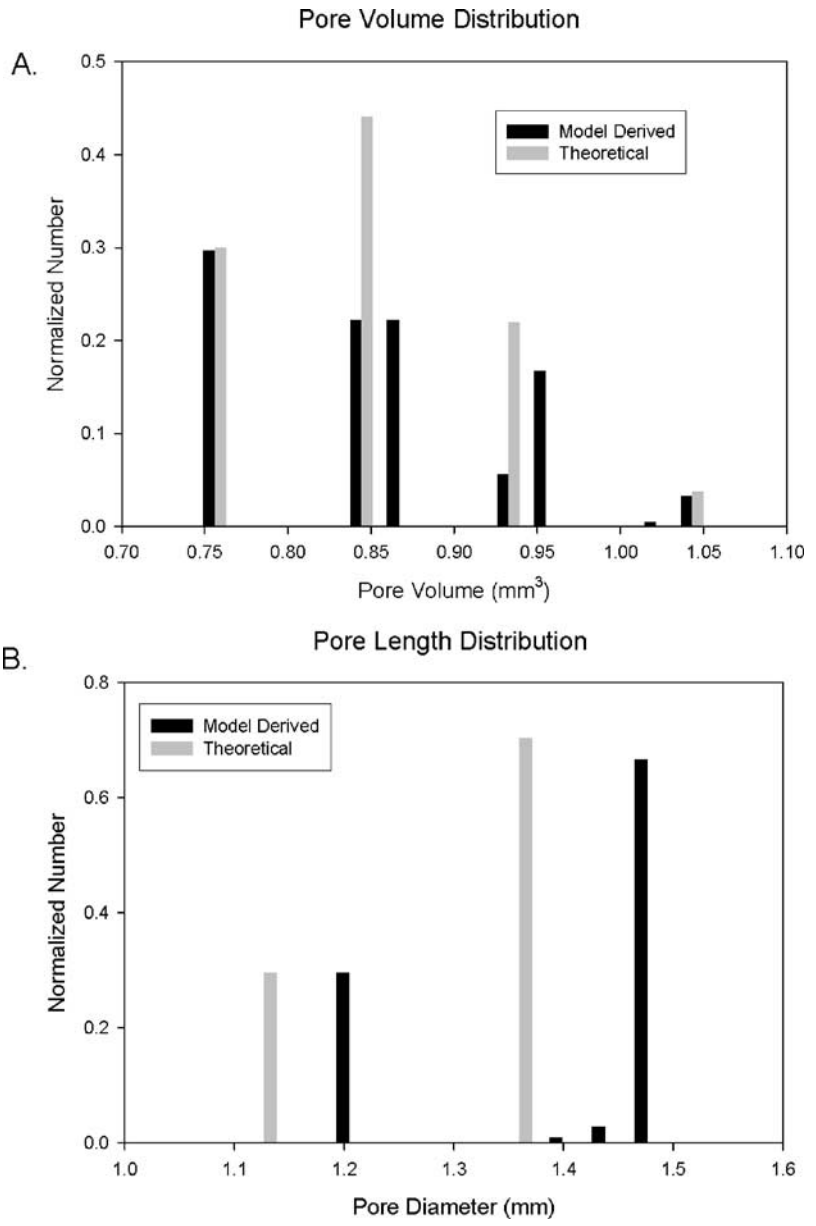

FIG. 3—*Comparison of theoretical and model derived histograms for the CWRU scaffold. Pore volume distribution (A), pore length distribution (B).*

TABLE 2—*Comparison of total pore volumes and number of objects in from quantitative analysis.*

	x, *y*, *z* Dimensions (mm)	Actual Number of Objects/ Expected Number of Objects
Theoretical	7.1, 7.1, 7.1	216/216
Model Derived	7.1, 7.1, 7.1	216/216
Part #2	7.06, 7.06, 5.91	186/180
Part #4	7.06, 7.06, 5.93	185/180
Part #17	7.04, 7.04, 5.92	183/180

ordering part 4 < part 17 < part 2 would be retained despite the choice of bin widths. This proved to be the case for the PV estimates cited here. Only reasonable binning schemes were used employing a modest number of bins and providing complete coverage of the data. However, because the variational distance values can be sensitive to the scheme used, it is important when computing variational distances for comparisons to maintain the same scheme for all items to be compared.

χ^2 for Uniformity Assessment—To assess the uniformity (consistency) of total pore volume, mean pore volume, and mean pore lengths across all parts, we employ a standard chi-squared type statistic:

$$\chi^2 = \sum \frac{(Observed - Expected)^2}{Expected} \tag{3}$$

where for *Expected* we use the average of the observed statistics, and for *Observed* we use the values of the individual empirically observed values. Values close to zero are indicative of uniformity. We do not perform formal inference on these values; we simply use the numbers as indicators of uniformity.

Results and Discussion

A three-dimensional model of the Type 1 scaffold was constructed from the CAD template and is shown in Fig. 1. Construction and analysis of a model scaffold is necessary to extract any intrinsic PV or PL distribution. The scaffold is 7.1 mm on each side, with the pore and strut lengths specified to be 600 μm and 500 μm, respectively. The Type 1 scaffold has 216 pores distributed into four distinct unit cell types found by Blob3D which are shown in Fig. 2. Table 1 gives a summary of the theoretical and model derived unit cell characteristics.

The theoretical values are calculated based on the expected dimensions of the pore. The unit cell is comprised of the cubic pore volume plus the volume that extends halfway into the strut. These characteristics were used to construct the theoretical PV and PL histograms shown in Fig. 3 to which the model derived and experimental data are compared. Figure 2(*a*) shows a unit cell from the scaffold interior—there are 64 such unit cells. Figure 2(*b*) displays a unit cell having one long axis. There are 96 of this type, which are found on the face of the cube. There are 48 unit cells of the type displayed in Fig. 2(*c*) that are present on the edges of the cube. Lastly, there are eight unit cells of the type shown in Fig. 2(*d*) that are found on each corner of the scaffold. The theoretical total pore volume (TPV) is 51.1 %, which is computed by summing the volumes of the individual unit cells and dividing by the total volume of the reference scaffold. Individual unit cell volumes are computed by summing the unit cell voxels. The TPVs are shown in Table 2 for theoretical, model-derived, and manufactured scaffolds. Table 2 contrasts the actual number of objects found with the expected number of objects, which gives an indication of the number of defects in the scaffold. The image sets from the manufactured scaffolds were cropped to a 6 by 6 by 5 pore dimension for analysis. The expected number of objects is 180. The results from Table 2 indicate that there are very few defects in the manufactured parts.

Next, the PV and PL of the unit cells were calculated from the model-derived structure using the Blob3D program. This was done to investigate whether the Blob 3D software introduced any bias into the results. Included in Table 1 are the number of unit cells for each type and the PV and PL outputs from the program, referred to as the "Model-Derived" values. Figure 3 displays the data of Table 1 in histogram form. Figures 3(*a*) and 3(*b*) show the PV and PL histograms comparing the theoretical and model-derived values. These figures provide insight into the intrinsic distributions of PV and PL. In Fig. 3(*a*), the model-derived pore volume is computed by simply summing the voxels of each unit cell. The volumes are

TABLE 3—*Comparison of structural descriptors for theoretical, model derived, and manufactured scaffolds.*

	Theoretical	Model Derived	Part 2	Part 4	Part 17
Total Pore Volume (%) (relative uncertainty, $\pm 1\sigma$)	51.1	51.1	50.0±1.47	50.8±1.47	52.6±1.47
Total Pore Volume Uniformity (mm^3) (χ^2)	…		0.0694		
Mean Pore Volume (mm^3) ($\pm 1\sigma$)	0.846±0.074	0.846±0.074	0.800±0.143	0.808±0.159	0.851±0.115
Pore Volume Uniformity (mm^3) (χ^2)	…		1.83×10^{-4}		
Variational Distance to theoretical (PV) ($\pm 1\sigma$)	…	0.039±0.020	0.158±0.035	0.087±0.025	0.146±0.031
Mean Pore Length (mm) ($\pm 1\sigma$)	1.28±0.11	1.36±0.129	1.45±0.19	1.44±0.23	1.45±0.22
Pore Length Uniformity (mm) (χ^2)	…		4.63×10^{-5}		
Variational Distance to theoretical (PL) ($\pm 1\sigma$)	…	0.700±0.022	0.708±0.040	0.671±0.033	0.670±0.033
Variational Distance to model (PL) ($\pm 1\sigma$)	…		0.477±0.04	0.419±0.033	0.474±0.038

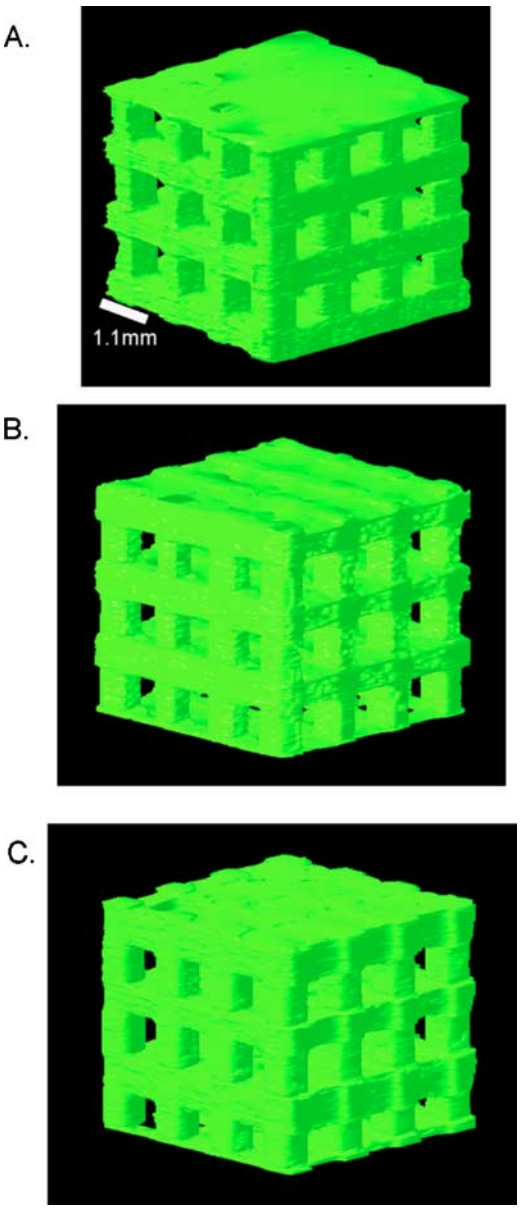

FIG. 4—*Reconstructions of X-ray CT images from selected parts. Subsections are presented for visual clarity. Part #2 (A), Part #4 (B), Part #17 (C).*

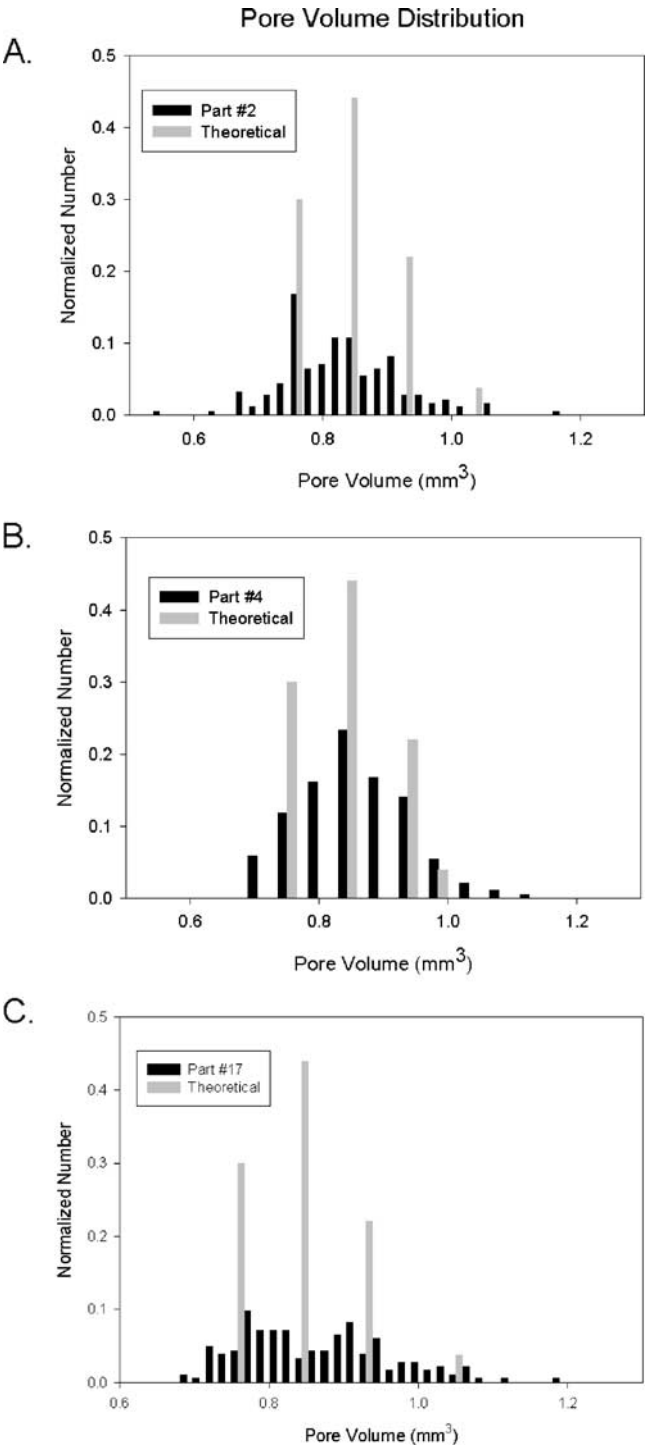

FIG. 5—*Pore volume distribution for Parts #2 (A), #4 (B), and #17 (C).*

then normalized by the total pore volume. As is evident from the figure, the model-derived PV distribution agrees well with the theoretical results. The PL values are taken from the longest axis of an ellipsoidal fit to each unit cell. Figure 3(*b*) displays the PL histograms, showing a systematic increase in results from theoretical to model values. These results suggest that while the software does a good job of computing PVs, the PL distribution for the model-derived PLs is about 7 to 9 % larger than the theoretical profile. This inflation in the model values originates from the way PL is computed. We have confirmed through visualization that the ellipsoid consistently extends slightly beyond the end of the unit cell as it attempts to optimize its long and short axis fit to the unit cell.

Figure 4 shows subsections of reconstructions from micro-CT imaging of three scaffolds manufactured by rapid prototyping. Qualitative comparison of these images to the model scaffold in Fig. 1 shows reasonable agreement in size and shape of the pores. Figure 5 compares the PV distributions from the three parts to the theoretical PV distribution. All distributions can be qualitatively described as clustering evenly around the theoretical modes with a slight tailing towards larger volumes. The three model-derived PL distributions in Fig. 6 are also skewed to larger PL when compared to the theoretical, and do a poorer job of capturing the theoretical frequencies. In this figure, clustering of bins occurs around the smaller PL value of about 1.2 mm (interior pores of Type A only) when compared to the model. This shows that the data from the parts agree well with the model, both undergoing similar inflation

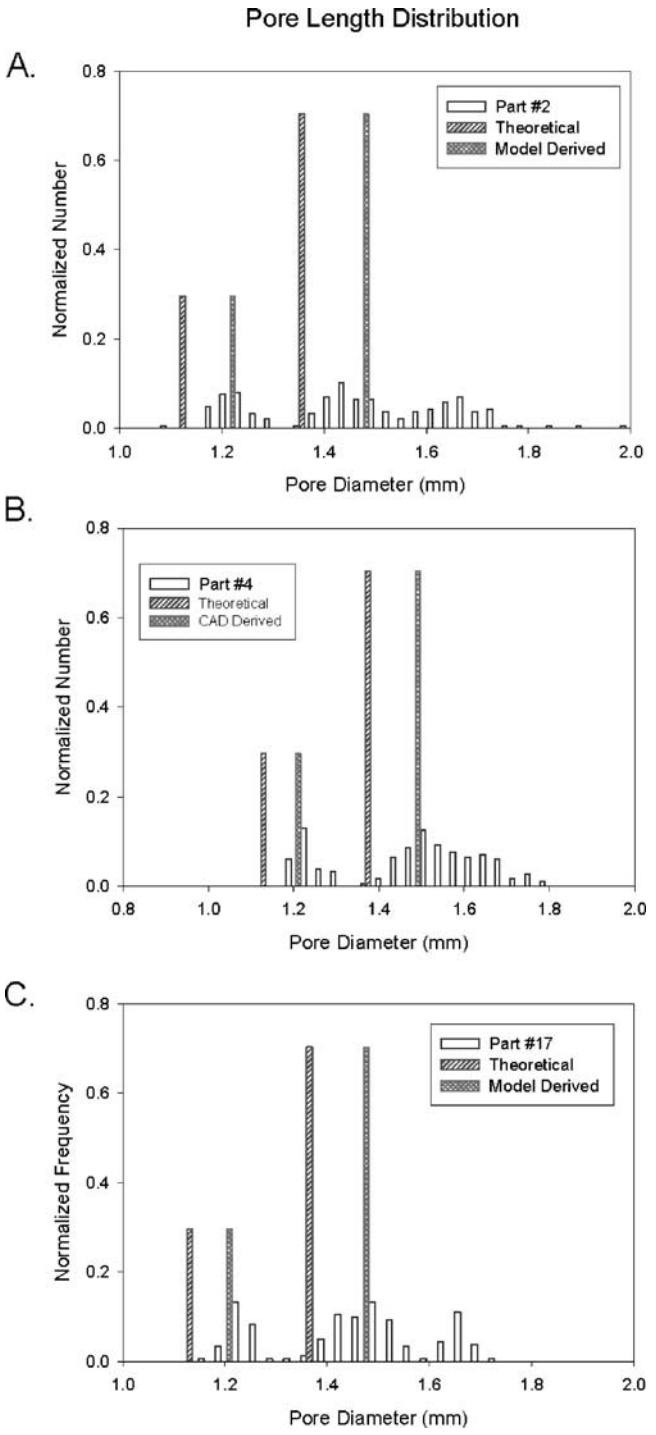

FIG. 6—*Pore length distribution for Parts #2 (A), #4 (B), and #17 (C).*

in PL when compared to the theoretical value. The PLs from the pores that are located on the surface of the scaffold (Types B, C, and D) are reflected in the larger bin at about 1.5 mm. There is also clustering of lengths around the model bin and also a tail that extends to larger values. A review of the individual pore image data shows that, for pore types C and D, the ellipsoid may not fit exactly to one axis, but will bisect the axes of similar length, resulting in a length longer than what is expected and is expressed as the tail in the data. This effect will diminish when the scaffold gets larger, and the number of interior pores increases relative to the exterior pores.

Statistical analysis of the histograms in Figs. 5 and 6 is given in Table 3 where the TPV, mean PV, mean PL, and the variational distance based on PV and PL are provided. Chi-squared (χ^2) is a relative measure of uniformity among the parts and is compared to uniformities from other types of scaffolds. This comparison is done in previous work [19]. Theoretical and model derived TPV match the TPVs from the manufactured parts within the specified uncertainties. For the manufactured parts, the mean PV for the unit cells is within one standard deviation of the theoretical mean value. The good fidelity of the scaffolds to the model is reflected in the low variational distances for PVs. The mean pore lengths for all parts are about 6 % larger than for the model-derived scaffold and about 12 % larger than for the theoretical value. This leads to a relatively large variational distance ($\approx$0.7) when the part and model distributions are compared to the theoretical. To take into account the bias introduced by the software, the variational distance is computed by comparing the parts to the model. The variational distance to the model-derived values for PL is still in the range of 0.4 to 0.5. The tailing of the distribution toward larger PLs contributes to the magnitude of the variational distance. It should be noted that the intrinsic PV distribution for a 6 by 6 by 5 pore scaffold is slightly different than for the model 6 by 6 by 6 scaffold to which the parts are being compared. The mean PV is 0.852 for a theoretical 6 by 6 by 5 scaffold. This has no impact other than to slightly elevate the PV variational distance. There is no corresponding change in the distribution for PL.

Conclusions

In this work, we have developed a methodology for evaluating the quality of candidate reference scaffolds. This methodology involves calculating three characteristics of interest: total pore volume, pore volume distribution, and pore length distribution. We calculate statistical measures of uniformity, standard uncertainty, and variational distance to evaluate the quality of the parts with respect to the theoretical and model values. We found the image quantitation software overestimates the pore lengths for the model-derived values for this particular scaffold geometry when compared to the theoretical values. The PL agreement of Parts #2, #4, and #17 to the model-derived values is good for the interior pores. Deviations from agreement with the model occur at the larger PL for the surface pores Type C and D because of additional difficulty fitting the long axis of pores on edges and at corners. This methodology indicates that total pore volume and pore volume distribution are the most reliable measures of scaffold quality, and that all three parts have total pore volumes and mean pore volumes statistically indistinguishable from the theoretical and model-derived values. The variational distance for the pore volume distribution is low for all three parts, confirming that it is close to the model.

References

[1] Tesk, J. A., "Special Report: NIST Workshop on Reference Data for the Properties of Biomaterials," *J. Biomed. Mater. Res.*, Vol. 58, No. 5, 2001, pp. 463–466.

[2] Tesk, J. A. and Karam, L. R., "NIST and Standards for Tissue Engineered Medical Products," *ASTM STP 1452*, E. Schutte, G. L. Picciolo, and D. S. Kaplan, Eds., 2003, ASTM International, West Conshohocken, PA.

[3] Tesk, J. A., "ASTM Task Force Open for Development of Reference Scaffolds for Tissue Engineering," *Biomaterials Forum*, Vol. 1st Quarter, 2004, p. 14.

[4] Jabbari, E., Lee, K. W., Ellison, A. C., Moore, M. J., Tesk, J. A., and Yazemski, M. J., "Fabrication of Shape Specific Biodegradable Porous Polymeric Scaffolds with Controlled Interconnectivity by Solid Free-form Microprinting," *Proceedings of 7th World Biomaterials Congress*, 2004, p. 1348.

[5] Cooke, M. N., Fisher, J. P., Dean, D., Rimnac, C., and Mikos, A. G., "Use of Stereolithography to Manufacture Critical-sized 3D Biodegradable Scaffolds for Bone Ingrowth," *J. Biomed. Mater. Res.*, Vol. 64B, No. 2, 2003 pp. 65–69.

[6] Khalil, S., Nam, J., and Sun, W., "Multi-nozzle Deposition for Construction of 3D Biopolymer Tissue Scaffolds," *Rapid Prototyping J.*, Vol. 11, No 1, 2005 pp. 9–17.

[7] Yeong, W. Y., Chua, C. K., Leong, K. F., and Chandrasekaran, M., "Rapid Prototyping in Tissue Engineering: Challenges and Potential," *Trends Biotechnol.*, Vol. 22, No 12, 2004, pp. 643–652.

[8] Hutmacher, D. W., Sittinger, M., and Risbud, M. V., "Scaffold-based Tissue Engineering: Rationale for Computer-aided Design and Solid Free-form Fabrication Systems," *Trends Biotechnol.*, Vol. 22, No. 7, 2004, pp. 354–362.

[9] Leong, K. F., Cheah, C. M., and Chua, C. K., "Solid Free-form Fabrication of Three-dimensional Scaffolds for Engineering Replacement Tissues and Organs," *Biomaterials*, Vol. 24, No. 13, 2003, pp. 2363–2378.

[10] Yang, S., Leong, K. F., Du, Z., and Chua, C. K., "The Design of Scaffolds for Use in Tissue Engineering. Part II. Rapid Prototyping Techniques," *Tissue Eng.*, Vol. 8, No. 1, 2002, pp. 1–11.

[11] Basu, S., Cunningham, L. P., Pins, G. D., Bush, K. A., Taboada, R., Howell, A. R., Wang, J., and Campagnola, P. J., "Multiphoton Excited Fabrication of Collagen Matrixes Cross-linked by a Modified Benzophenone Dimer: Bioactivity and Enzymatic Degradation," *Biomacromolecules*, Vol. 6, No. 3, 2005, pp. 1465–1474.

[12] Ho, S. T. and Hutmacher, D. W., "A Comparison of Micro CT With Other Techniques Used in the Characterization of Scaffolds," *Biomaterials*, Vol. 27, No. 8, 2005, pp. 1362–1376.

[13] Moore, M. J., Jabbari, E., Ritman, E. L., Lu, L., Currier, B. L., Windebank, A. J., and Yaszemski, M. J., "Quantitative Analysis of Interconnectivity of Porous Biodegradable Scaffolds with Micro-computed Tomography," *J. Biomed. Mater. Res. A*, Vol. 71, No. 2, 2004, pp. 258–267.

[14] Sodian, R., Fu, P., Lueders, C., Szymanski, D., Fritsche, C., Gutberlet, M., Hoerstrup, S. P., Hausmann, H., Lueth, T., and Hetzer, R., "Tissue Engineering of Vascular Conduits: Fabrication of Custom-made Scaffolds Using Rapid Prototyping Techniques," *Thorac. Cardiovasc. Surg.*, Vol. 53, No. 3, 2005, pp. 144–149.

[15] Lin, A. S., Barrows, T. H., Cartmell, S. H., and Guldberg, R. E., "Microarchitectural and Mechanical Characterization of Oriented Porous Polymer Scaffolds," *Biomaterials*, Vol. 24, No. 3, 2003, pp. 481–489.

[16] Cartmell, S., Huynh, K., Lin, A., Nagaraja, S., and Guldberg, R., "Quantitative Microcomputed Tomography Analysis of Mineralization Within Three-dimensional Scaffolds in Vitro," *J. Biomed. Mater. Res. A*, Vol. 69, No. 1, 2004, pp. 97–104.

[17] Jones, A. C., Milthorpe, B., Averdunk, H., Limaye, A., Senden, T. J., Sakellariou, A., Sheppard, A. P., Sok, R. M., Knackstedt, M. A., Brandwood, A., Rohner, D., and Hutmacher, D. W., "Analysis of 3D Bone Ingrowth into Polymer Scaffolds via Micro-computed Tomography Imaging," *Biomaterials*, Vol. 25, No. 20, 2004, pp. 4947–4954.

[18] Blom, G., Holst, L., and Sandell, D., *Problems and Snapshots From the World of Probability*, Springer-Verlag, New York, NY, 1994.

[19] Dunkers, J. P., Leigh, S. D., Cicerone, M. T., Landis, F. A., Wang, F., and Tesk, J. A., "NIST Development Of Reference Material Scaffolds for Tissue Engineering," *Proceedings of IMECE 2005: 2005 ASME International Mechanical Engineering Congress and Exposition*, 2005, Abs. No. 82012.

[20] Ketcham, R. A., "Computational Methods for Quantitative Analysis of Three-Dimensional Features in Geological Specimens," *Geosphere*, Vol. 1, No. 1, 2005 pp. 32–41.

[21] DATAPLOT:http://www.itl.nist.gov/div898/software/dataplot.

[22] Efron, F. B. and Tibshirani, R. J., *Introduction to the Bootstrap*, Chapman and Hall, New York, NY, 1993.